REPORT DOCUMENTATION PAGE

Form Approved
OMB NO. 0704-0188

1. AGENCY USE ONLY (Leave Blank)	2. REPORT DATE	3. REPORT TYPE AND DATES COVERED
	July 20, 2005	Final Report August 15, 2000-April 14, 2004

4. TITLE AND SUBTITLE
A Study to uncover the Microstructural Basis for the Intrinsic Toughness of Interfaces and its Relation to the Plastic work that Accompanies Interface Decohesion

5. FUNDING NUMBERS
DAAD19-00-1-0491

6. AUTHOR(S)
Vijay Gupta

7. PERFORMING ORGANIZATION NAME(S) AND ADDRESS(ES)
Department of Mechanical and Aerospace Engineering, UCLA, Los Angeles, CA 90095

8. PERFORMING ORGANIZATION REPORT NUMBER

9. SPONSORING / MONITORING AGENCY NAME(S) AND ADDRESS(ES)
U. S. Army Research Office
P.O. Box 12211
Research Triangle Park, NC 27709-2211

10. SPONSORING / MONITORING AGENCY REPORT NUMBER
40925.1-MS

11. SUPPLEMENTARY NOTES
The views, opinions and/or findings contained in this report are those of the author(s) and should not be construed as an official Department of the Army position, policy or decision, unless so designated by other documentation.

12 a. DISTRIBUTION / AVAILABILITY STATEMENT
Approved for public release; distribution unlimited.

12 b. DISTRIBUTION CODE

13. ABSTRACT (Maximum 200 words)

A fundamental relationship between intrinsic and total toughness of tantalum/sapphire, Al/epoxy, and Si/epoxy joints is established using several novel interface characterization tools. The focus of research was to understand issues related to size effects, energy absorption capacity, and reliability, of joints. A double cantilever beam experiment equipped with a cryogenic cell, and a laser-generated stress wave technique was used to measure the strength and toughness of interfaces, respectively. Although not part of the original proposal, experimental procedures to determine interfacial moisture content were established and then related to the measured interface strength. This was demonstrated for a polymer/nitride interface. This allows quantitative prediction of the durability of epoxy joints in service. The experimental procedures are general and applicable to epoxy/Al joints of direct interest to the Army. In addition, a novel application of laser-generated stress waves was developed which involved their use in releasing stiction in MEMS devices. Finally, during the execution of the above research objectives, discovery of glass modified stress waves with rarefaction shocks was made. The technological importance of such waves in measuring the interfacial tensile strength of ultrathin films was demonstrated. The ability of the glass to modify the rise time of the stress pulse from 1-2 ns to almost 50 ns points to an interesting effect that is worthy of further inquiry for defeating shock fronts for the purposes of designing armors.

14. SUBJECT TERMS
Adhesion, Laser Spallation, Composite Joints, Humidity, MEMS, Stiction, Intrinsic Toughness, Total Toughness, Intrinsic Strength, Rarefaction Shock, Shock Waves.

15. NUMBER OF PAGES
30

16. PRICE CODE

17. SECURITY CLASSIFICATION OR REPORT	18. SECURITY CLASSIFICATION ON THIS PAGE	19. SECURITY CLASSIFICATION OF ABSTRACT	20. LIMITATION OF ABSTRACT
UNCLASSIFIED	**UNCLASSIFIED**	**UNCLASSIFIED**	**UL**

TABLE OF CONTENTS **Page Number**

List of Illustrations and Tables

I. Statement of Problem Studied

There were several aims of the proposed work:

(1) Fabricate 6061-T6 Aluminum/Epoxy, (2) Tantalum/Sapphire, and (3) Epoxy/Si joints using novel chemical and mechanical routes, (2) characterize the fundamental interface mechanical properties of intrinsic tensile strength, intrinsic toughness, and total toughness using novel experiments, and (3) experimentally determine the relationship among the latter to understand issues related to size effects, energy absorption capacity, and reliability, of the Tantalum/Sapphire and epoxy joints.

Although not part of the original proposal, experimental procedures to determine interfacial moisture content were established and then related to the measured interface strength. This was demonstrated for a polymer/nitride interface. This allows quantitative prediction of the durability of epoxy joints in service. In addition, two novel applications of laser-generated stress waves were also developed. The first was their use in cavitating human adipose tissue (fat). This was caused by raising the cell's internal hydrostatic pressure by the stress waves. The second application involved their use in releasing stiction in MEMS devices.

Finally, during the execution of the above research objectives, discovery of glass modified stress waves with rarefaction shocks was made. The technological importance of such waves in measuring the interfacial tensile strength of ultrathin films (less than 0.1 micrometers in thickness) was also demonstrated. Some of the research results discussed here were also reported in the final report for the ARO equipment Grant No. DAAD19-02-1-0157, that paralleled and complemented the present grant.

Results pertaining to each of the above research activities are discussed below.

II. Technical Approach

Silane-based chemistries were used to bond the joint sections. The goal was to optimize adhesion since each joint is presently being used in a mechanical stress environment. Interfaces were also weakened so as to generate total toughness data for different levels of intrinsic toughness. This was useful in understanding the poorly understood nonlinear relationship between the intrinsic and total interface toughness, which was the main thrust of the proposed research.

The total toughness was measured using a double cantilever beam experiment. This setup was also equipped with an environmental cell so as to allow toughness measurements at cryogenic temperatures. The idea was to progressively reduce the plastic component (because of the yield strength dependence on temperature) of the deformation during interface separation such that the measured toughness values will approach those of the intrinsic toughness at the lowest temperature. Figures 1 and 2 show the DCB setups. Details of the experimental procedures and test setup can be found in Wang [1] and articles that have been already accepted or published from the support of this grant [2-4].

The intrinsic strength was measured using a laser-induced stress wave experiment. In this experiment, a 16 to 20 nanoseconds long pressure pulse is generated in the substrate plate (here Al, sapphire, and Si) towards the second layer (here epoxy, and tantalum) bonded (or deposited) on its top face. The pressure pulse reflects into a tensile wave from the free surface of the second layer and loads the interface in tension. The interface separates if the tensile stress exceeds the joint strength. Figure 3 shows the schematic of the setup, with details and experimental procedures described in [1-4].

The above apparatuses were used to determine both the intrinsic strength and intrinsic and total toughnesses for all the three joints.

III. Results

3.1. Effects of Substrate Orientation and Metal Film Thickness on the Intrinsic Strength, Intrinsic Fracture Energy, and Total Fracture Energy of Tantalum-Sapphire Interfaces

Specifically we developed relationships between total fracture energy (G_c) and intrinsic fracture energy (G_o), and between intrinsic tensile strength (σ_o) and G_o, for interfaces between sputter-deposited polycrystalline tantalum coatings and sapphire substrates, by using experimental procedures discussed above. Relationships among these parameters for the same system have never been accomplished before. Besides serving as a model system for a general metal/ceramic couple, such interfaces are of direct interest in the development of multilayer metal/ceramic nanolaminates for use in newer types of lightweight armors. In addition to being controlled by the intrinsic toughness, G_c depends upon many extrinsic parameters such as the yield strengths of the substrate and coating materials, coating/substrate geometry, and the type of loading (strain rate, temperature, and the far-field mode I to mode II stress ratio), among others. To keep the research focused, only the effects of sapphire surface orientation, temperature, and metal layer thickness on the intrinsic-to-total toughness relationship was studied. The intrinsic toughness and strength were modified by changing the orientation of the sapphire surface (basal and prismatic), while G_p was varied by changing the test temperature (ambient and cryogenic) and the thickness (1, 2, and 3 μm) of the ductile Ta layer. The double cantilever beam (DCB) experiment (Fig. 1) was used to measure G_c, while G_o was obtained by carrying out the DCB tests at the cryogenic temperature (Fig. 2). The laser spallation experiment was used to measure the tensile strength of the interface (Fig. 3).

Table I and Figure 4 summarizes all the measurements and the relationships among the various parameters. Several points are noteworthy. For the specimens bearing the same film thickness and tested at the same temperature, interfaces with the basal sapphire surface orientation exhibited a higher G_c values than those involving the prismatic sapphire surface

orientation. This is consistent with the corresponding G_o and σ_o values, indicating that the plastic contribution is controlled directly by the details of the local atomic bonding.

The different surface structures of the two types of substrates, simulated using the Crystal Kit program, are shown in Fig. 5. Fig. 5(a) shows the atoms on a C-plane sapphire substrate surface, terminated by an O layer. The figure shows that the surface oxygen atoms on the C-plane sapphire substrate are all singly bonded. These singly bonded surface oxygen atoms can readily bond with the Ta atoms in the coating. Fig. 5(b) shows an O-terminated A-plane sapphire surface. Here, only two thirds of the surface oxygen atoms are singly bonded. Thus, the C-plane sapphire has a higher density of adsorption sites for metal atoms to form metal-O bonds, which explains why C-plane substrate samples have a higher interfacial strength.

Figure 4 shows that G_c increases with increasing tantalum coating thickness for a fixed G_o for both types of interfaces. The increased metallic layer thickness provides a larger material volume to deform under the influence of crack-tip stresses. The data for both orientations show a tendency towards saturation. This is expected since eventually the plastic deformation processes should be terminated when the local crack tip stresses are sufficient to provide the necessary G_o or σ_o for interface decohesion.

The interface strength for both orientations is quite low. This is probably due to interfacial defects. However, in spite of these low values, the interface strength trend is consistent with the measured G_o values. A previously derived relationship between G_o and σ_o based on universal bonding correlation suggests a direct correlation between these parameters.

For both orientations, the plastic deformation at each film thickness has not attained a saturated value of G_p as the latter increases when the film thickness is increased. Apparently G_o is too low to utilize the full plastic capacity of the structure. This capacity seems to be nearing for both orientations at a Ta film thickness of about 3 μm. This is expected since eventually the plastic deformation process will be terminated when the local crack tip stresses are sufficient to

provide G_o or σ_o for interface decohesion. Once this state has been reached any extra Ta volume will remain essentially unutilized.

For each orientation, value of G_o has been measured. This is because at 77K plastic deformation in Ta and other materials in the vicinity of the interface is essentially frozen. This is consistent with the observed independence of the measured G_o value with the thickness of the ductile Ta film. Comparing with the G_c values, G_o constitutes only a small fraction (12-13%).

The saturation effect also suggests the inadequacy of pure elasticity solutions in modeling the fracture behavior of metal/ceramic layered systems when their fracture energies near the 45 J/m^2 mark. Thus, systems characterized by such fracture energies are best modeled using elasto-plastic constitutive material laws in which the local crack advance conditions are set by G_o. Details of the above research are already published in [1].

3.2. Glass/Epoxy Interfaces

Of particular interest to this system was to measure the effects of interlayer chemistry on glass/epoxy interfaces. These samples were provided by Dr. Kent from the Sandia National Laboratories. The interlayer was in the form of a monolayer whose chemistry was varied in terms of the number and type of terminal groups. Methyl and Br-terminated monolayers with 50 and 100% coverage were considered. Epoxy chemistry was also changed. The measured interface strengths varied widely from 22 MPa to 288 MPa, depending upon the interfacial chemistry. These measurements prove yet again the ability of the laser spallation experiment to uncover the microstructural basis for the measured interface strengths. Given the limited scope of the work, no manuscript was prepared but the results were communicated to the Sandia National Laboratory.

3.3. Al/epoxy Joints

Fabrication of Al/epoxy joints, with and without silane, were fabricated, and the joint toughness evaluated using the double cantilever beam setup equipped with the cryogenic cell. The degrading effect of moisture was also evaluated, with results summarized in Fig. 6. Such results can be used in practice to determine the life of Al/epoxy joints.

3.4. A Quantitative Study of Moisture Adsorption in Polyimide and its Effect on the Strength of the Polyimide/Silicon-Nitride Interface

Polyimide films on silicon nitride substrates were exposed to moisture under varying conditions of relative humidity, time and temperature. The moisture content of the films was measured by FTIR spectroscopy (Fig. 7), and the polyimide/silicon nitride interface strength was measured at room temperature by a laser spallation technique. The moisture adsorption by polyimide films was analyzed using a diffusion model. Under the experimental conditions of this study, it was found that the rate of moisture adsorption was controlled the surface exchange reaction. For samples exposed at 38°C, the interface strength was found to decrease linearly with increasing interface moisture concentration (Fig. 8). A critical interface moisture concentration was identified, where the strength is expected to go to zero. The interface strengths of all the measured samples were combined into one empirical equation that can be used as a basis to construct strength charts as a function of exposure conditions. The concentration dependence of the interface strength S, according to this equation is given as:

$$(1) \qquad S = A\,(C_{crit} - C_I)\, e^{\frac{Q}{RT}}$$

where C_I implicitly represents the exposure time and relative humidity in this expression. A best fit of this equation to strength data obtained for all samples exposed to different time/temperature/humidity condition yielded, A = 1384 MPa and Q = 7300 J/mole K. Figure 9 shows a plot of experimental value of the interface strength *S* versus the calculated value of *S*

based on Eqn. 1. The figure shows the data points are reasonably close to the 45° line, which represents a perfect fit to the experimental data.

The strength charts defined by this equation should help in the development of more rational standards for handling packaged IC's during manufacturing and integration from the viewpoint of avoiding moisture-related failures. Details of theis research can be found in [2]. Also the procedures described in this research are general and applicable to Al/epoxy joints that have direct interest to the Army.

3.5. Summary of Most Important Results-IV: Recovery of Stiction-failed MEMS Structures using Laser-induced Stress Waves

Stiction, or adhesion between suspended structures and the underlying surface, is a hurdle in batch fabricating long, freestanding MEMS structures. A novel technique was developed to release stiction. In this technique (Fig. 10), a nanosecond rise time stress wave is launched on the backside of the Si substrate by impinging a 2.5 ns-duration Nd:YAG laser pulse onto a 3mm-dia area. The compressive stress wave propagates through the Si substrate and arrives at the site of several stiction-failed cantilevers on the front Si surface. The compressive stress wave propagates through the cantilevered structures and is reflected into a tensile wave from their free surfaces. The returning tensile wave pries off the interface, releasing the cantilevers. The procedure is demonstrated on a MEMS chip with stiction-failed cantilevers with varying lengths from 100 μm to 1000 μm. The threshold laser energy to release stiction increased linearly with cantilever lengths (Fig. 11). Beam recovery began at a laser fluence of 11 kJ/m^2 laser energy. 70% of the tested beams had been recovered after impingement with a fluence of 26 kJ/m^2. After the highest applied laser fluence of 40 kJ/m^2, 90% of the tested beams had been recovered. No damage to the structures or surrounding features was observed below 40 kJ/m^2. Because of rather low laser fluence, no thermal damage to the back surface of Si was noted. Since it literally takes few seconds to release stiction, the proposed technique can be implemented in MEMS foundry, and for repair of in-use stiction failed MEMS devices.

3.6. Discovery of Glass-Modified Stress Waves with Rarefaction Shocks

Observations of laser-generated stress wave profiles with rarefaction shocks (almost discontinuous or zero post-peak decay times) in glasses were uncovered. Figure 12 shows a series of stress pulse profiles with increasing laser fluence, measured in a soda lime glass. At low stress amplitudes, the profiles are similar to that in Si and other materials, having a finite (1-2 ns) rise-time and gradual post-peak decay (14-18 ns). However, as the stress pulse amplitude exceeds a certain threshold, the rise-time of the stress wave gets longer but the post-peak stress profile starts to decay rather quickly. Ultimately a profile is attained with the post-peak stress dropping instantaneously (the drop time is within the resolution limit of our instrumentation), much like a "rarefaction shock." The modification in the stress wave profile due to glass compared with that due to Si can be appreciated by viewing Fig 14a.

Figure 13 shows the pulse profiles measured in Pyrex, soda lime, quartz, and borosilicate glasses. The magnitude of the above effect was found to vary from glass to glass, but all showed the formation of the rarefaction shock.

The rarefaction shock stems from an initially increased compressibility of glass under increasing pressures. The decrease in the wave speed is evident in the increase in the rise-time of the stress wave with its amplitude (Fig. 12). Thus, the formation of rarefaction shock can be thought to occur due to overcrowding of the faster moving post-peak wave profile into the significantly decelerating pulse front.

The initial ramp-like behavior has been attributed to the nonlinear elastic response in glasses, which in turn, has been related to phase transformation and material densification (Barker and Hollenbach, 1970; Clifton, 1993).

Previous investigators (e.g., see, Clifton et al., 1997) who used plate impact setups were unable to uncover the formation of rarefaction shocks in glasses since the pulse lengths in their

work was larger than the specimen thickness. As suggested above, this effect develops due to finite propagation distance of the pulse into the material. This became possible in our work because of the short length (~0.1 mm) of the stress waves compared with the specimen thickness (~1 mm).

The technological importance of these pulses in measuring the tensile strength of very thin film interfaces has been demonstrated using the laser spallation experiment. Because of the rarefaction shock, glass-modified waves allow generation of substantially higher interfacial tensile stress amplitudes compared with those with finite post-peak decay profiles. This is demonstrated in Figure 14. Figure 14a shows the failure inside the Si in a Cu(1400nm)/TiN(70nm)/Si system when no glass was used. Figure 14b shows a high magnification view of failure caused by a wave generated inside the glass and transferred to the backside of the Si substrate. The arrow shows the failure to be at the Cu/TiN interface with no fracture inside the Si. An interface tensile strength value of 2.62 GPa was calculated. This is a rather high value, which was not possible to attain using the basic spallation setup for the film thicknesses tested. This is demonstrated in Figs. 14 c and (d). Figure 14 (c) shows the measured free surface velocity profiles in the borosilicate glass and Si substrates corresponding to the failures shown in Fig. 14 (a) and (b). The interface tensile stress history corresponding to each profile is shown in Fig. 14 (d). The dramatic increase in the interface tensile stress due to the glass-modified wave is evident.

Thus, for the first time, tensile strength of very strong and ultra thin film interfaces can be measured. Although a strong function of intrinsic strength, the results to date suggest testing of 185-nm-thick fims with interface strengths approaching 2.7 GPa. Thus, an important advance has been made that should allow material optimization of ultra thin layer systems that may form the basis of future MEMS-based microelectronic, mechanical and clinical devices.

IV. Publications

Papers published in peer-reviewed journals

1. "Effects of Substrate Orientation and Metal Film Thickness on the Intrinsic Strength, Intrinsic Fracture Energy, and Total Fracture Energy of Tantalum-Sapphire Interfaces," X. Wang, V. Gupta, S.N. Basu, J. American Ceramic Society, 88, 7 (2005) 1909-1913**.**

2. A quantitative study of moisture adsorption in polyimide and its effect on the strength of the Polyimide/Silicon-Nitride interface," A. Jain, V. Gupta and S.N. Basu, Acta Materialia, 53 (2005) 3147-3153.

3. "Rupture of fat cells using laser-generated ultra short stress waves," K. Kuwahara, H.B. Gladstone, V. Gupta, V. Kireev, V. Neel, and R.L. Moy, Lasers in Surgery and Medicine, **32**, 4 (2003) 279-285.

4. "The effect of structure and chemistry on the strength of FeCrAl(Y)/Sapphire interfaces: I, structure of interfaces," H. Wu, S.N. Basu, V. Kireev, and V. Gupta, Materials Science and Engineering A, **A349** (2003) 248-255.

5. "The Effect of structure and chemistry on the strength of FeCrAl(Y)/Sapphire interfaces: II, strength of interfaces," H. Wu, S.N. Basu, V. Kireev, and V. Gupta, Materials Science and Engineering A, **A349** (2003) 265-271.

6. "Glass-modified stress waves for adhesion measurement of ultra thin films for device applications," V. Gupta, V. Kireev, H. Yoshida, and H. Akahoshi, J. Mechanics and Physics of Solids, **51** (2003) 1395-1412.

7. "In-Situ intrinsic interface strength measurement at elevated temperatures and its relationship to interfacial structure," V. Gupta, V. Kireev, S.N. Basu, and H. Wu, Interface Science, **11** (2003) 359-368.

8. "Recovery of stiction-failed MEMS structures using laser-induced stress waves," V. Gupta, R. Snow, M.C. Wu, A. Jain, and J.C. Tsai, J. of Microelectromechanical Systems, **13**, 4 (2004) 696-700.

9. "Study of the interface strength of zirconia coatings by a laser spallation technique," A. Kobayashi, A. Jain, V. Gupta, and V. Kireev, Vaccum, **73** (2004) 533-539.

10. "Construction and characterization of chemically-joined stainless steel/E-glass composite sections," X. Wang and V. Gupta, Mechanics of Materials, in press (2005).

Papers published in non-peer-reviewed journals or in conference proceedings

11. "Measurement of solder joint strength and its dependence on thermal aging in freestanding and board-mounted packages using a laser spallation technique," V. Gupta, J. Tian, C. Hartfield, K. Zeng, C. Chiu, and R. Stierman, to appear in the Proc. of the 30th International Symposium for Testing and Failure Analysis 2004, Worcester, Massachusetts (2004), November 14-18.

12. "Novel applications of laser-generated stress waves in manufacturing of MEMS and ICs on plastics," V. Gupta, to appear in the Proc. of the 2005 NSF DMII Grantees Conference, Scottsdale, Arizona (2005), Jan 3-6.

Manuscripts submitted, but not published

13. "Measurement of the intrinsic and total fracture energies, and intrinsic strength of stainless steel/E-glass composite joints," X. Wang and V. Gupta, Journal of Adhesion Science and Technology, in review (2005).

V. Scientific Personnel Supported

Amit Jain-Ph.D Student.
Xuemei Wang (woman)-Ph.D. Student. Granted Ph.D. April, 2005.
Vassili Kireev-Post Doctoral Research Associate.
Jun Tian (woman)-Ph.D. Student. Granted Ph.D. in March 2005.

VI. Report of inventions

Title: Glass-modified stress waves for separation of untra thin films and nanoelectronics device fabrication. Filed March 2005. This application claims priority from U.S. provisional application serial number 60/550,803 that was filed on March 5, 2004, to the US Patent Office.

VII. Bibliography

1. "Effects of Substrate Orientation and Metal Film Thickness on the Intrinsic Strength, Intrinsic Fracture Energy, and Total Fracture Energy of Tantalum-Sapphire Interfaces," X. Wang, V. Gupta, S.N. Basu, J. American Ceramics Society, 88, 7 (2005) 1909-1913**.**

2. Wang, X., July 2004. Chemical Construction, Mechanical Characterization and Durability of Metal and Composite Structural Joints, Ph.D. Dissertation, Department of Mechanical and Aerospace Engineering, UCLA, Los Angeles, CA.

3. "A quantitative study of moisture adsorption in polyimide and its effect on the strength of the Polyimide/Silicon-Nitride interface," A. Jain, V. Gupta and S.N. Basu, Acta Materialia, 53 (2005) 3147-3153.

4. "Construction and characterization of chemically-joined stainless steel/E-glass composite sections," X. Wang and V. Gupta, Mechanics of Materials, in press (2005).

5. "Shock-wave studies of PMMA, fused silica, and sapphire," L. M. Barker and R.E. Hollenbach, J. Appl. Physics, 41, 10 (1970) 4208-4226.

6. "Effect of shear on failure waves in soda lime glass," R. J. Clifton, M. Mello, N.S. Brar. Shock Compression of Condensed Matter-1997. The American Institute of Physics, New York, pp. 521-524.

Table I. Fracture energies, G_c, for specimens with different sapphire surface orientations (basal and prismatic) and tantalum film thickness obtained at ambient and cryogenic temperatures. Also shown are the tensile strength values, σ_0, of the Ta/sapphire interface measured using the laser spallation experiment.

Sapphire surfaces	Film thickness (μm)	G_c (J/m^2)	G_0 (J/m^2)	σ_0 (MPa)
Basal	1	20.5 ± 1.5	5.8 ± 0.6	279 ± 18
	2	39.7 ± 5	5.5 ± 0.5	
	3	43.4 ± 3		
Prismatic	1	15.9 ± 2	4.7 ± 0.5	142 ± 10
	2	33.9 ± 5	5.0 ± 0.6	
	3	40.4 ± 5		

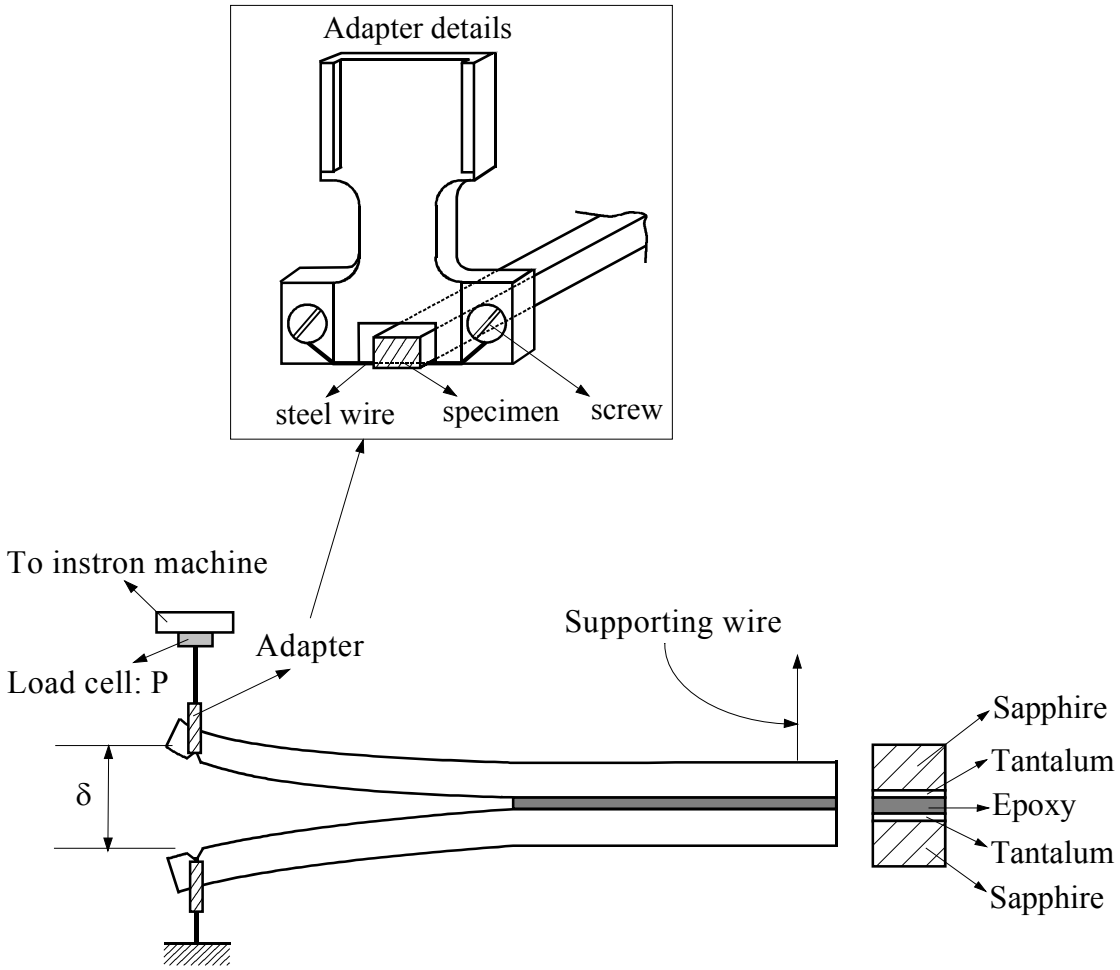

Figure 1. Schematic of the double cantilever beam experiment along with that of the cross-section of a typical specimen. The inset shows the details of the adapter design and how it secures the end of the beam to avoid slippage during testing.

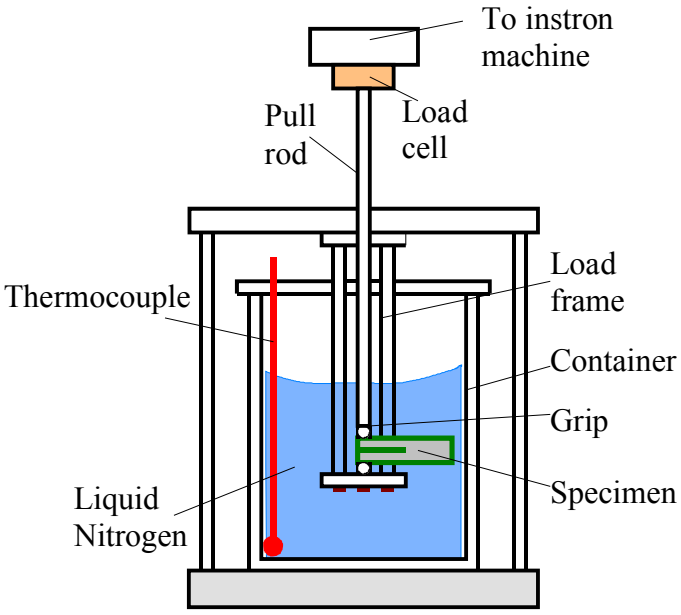

Figure 2. Schematic of the setup used for measuring the intrinsic fracture energy of the interface. The double cantilever beam test is essentially done at the liquid nitrogen temperature of 77 K.

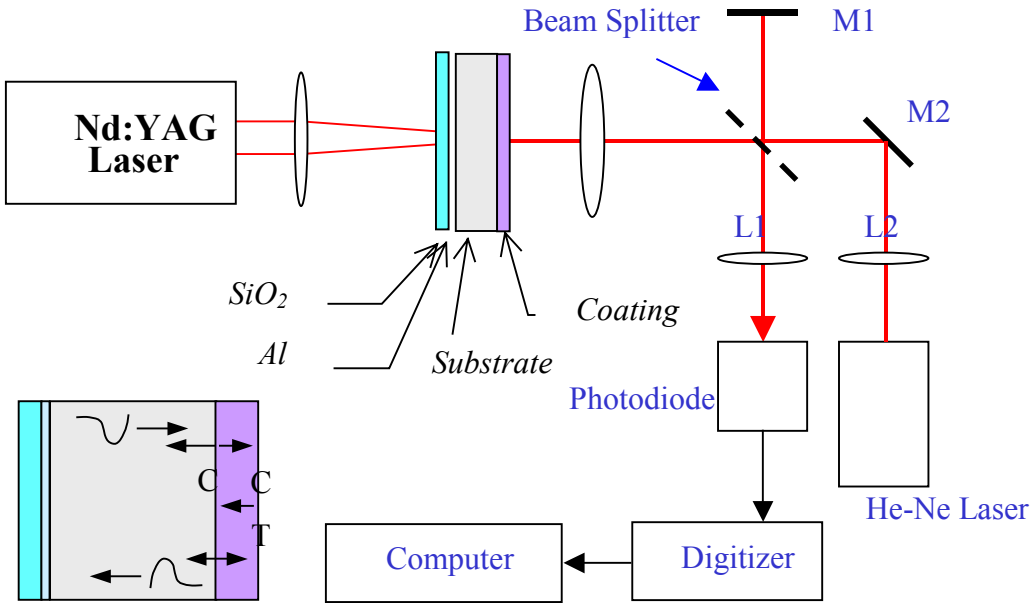

Figure 3. Schematic of the laser spallation experiment along with that of an interferometer used to quantify the stress waves in the sapphire substrate.

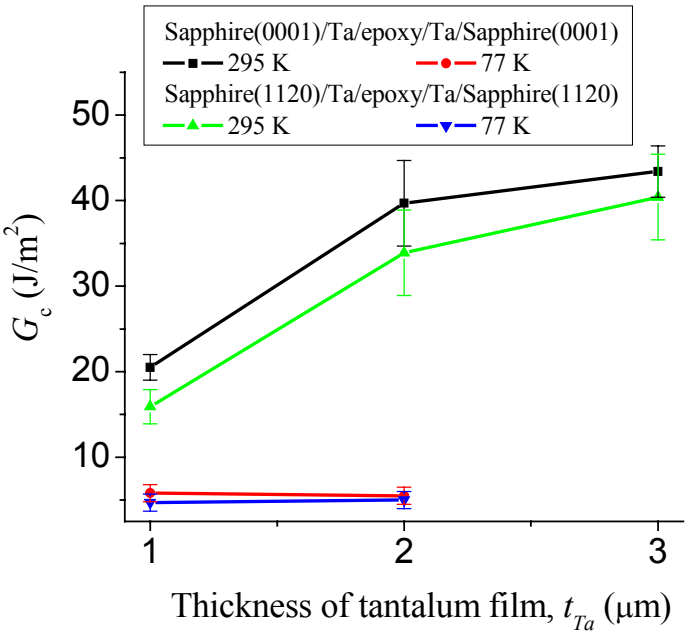

Figure 4. Fracture energies, G_c, for specimens with different sapphire surface orientations (basal and prismatic) and tantalum film thickness obtained at ambient and cryogenic temperatures.

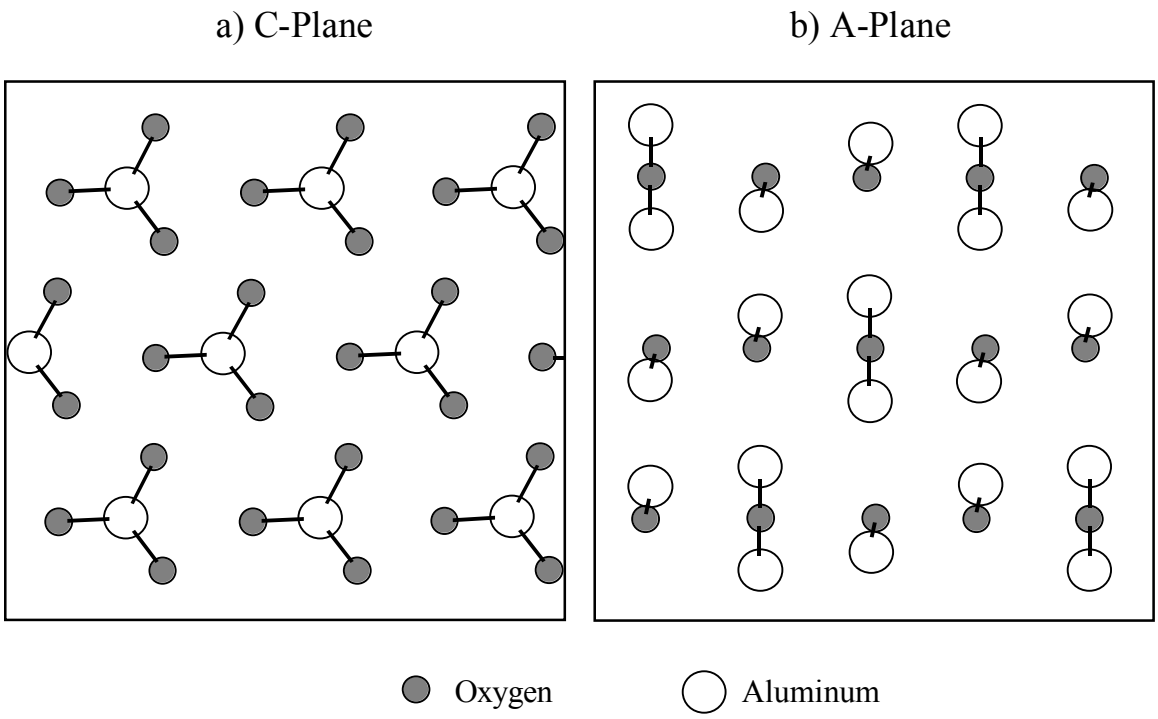

Figure 5. Oxygen-aluminum bonds in oxygen-terminated surfaces in a) C-plane and b) A-plane sapphire. All the oxygen atoms in the C-plane surface and only two-thirds of the atoms in the A-plane surface are singly bonded and are potential sites for bonding with Ta atoms.

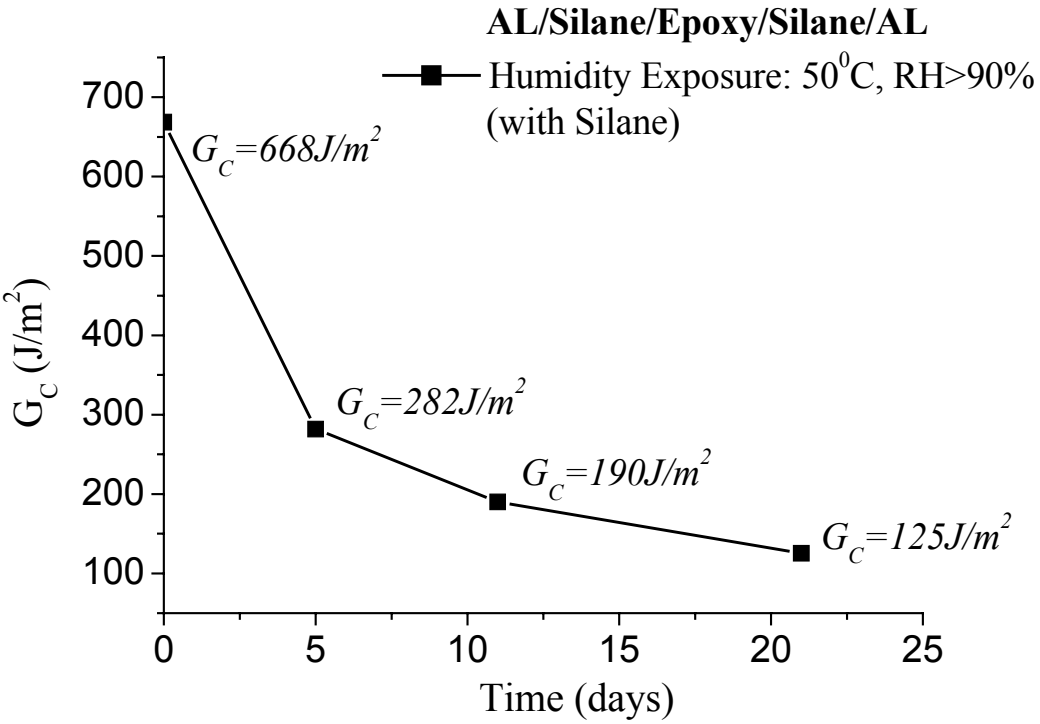

Figure 6. Effect of humidity on the total toughness of Al/silane/epoxy/silane/Al joints.

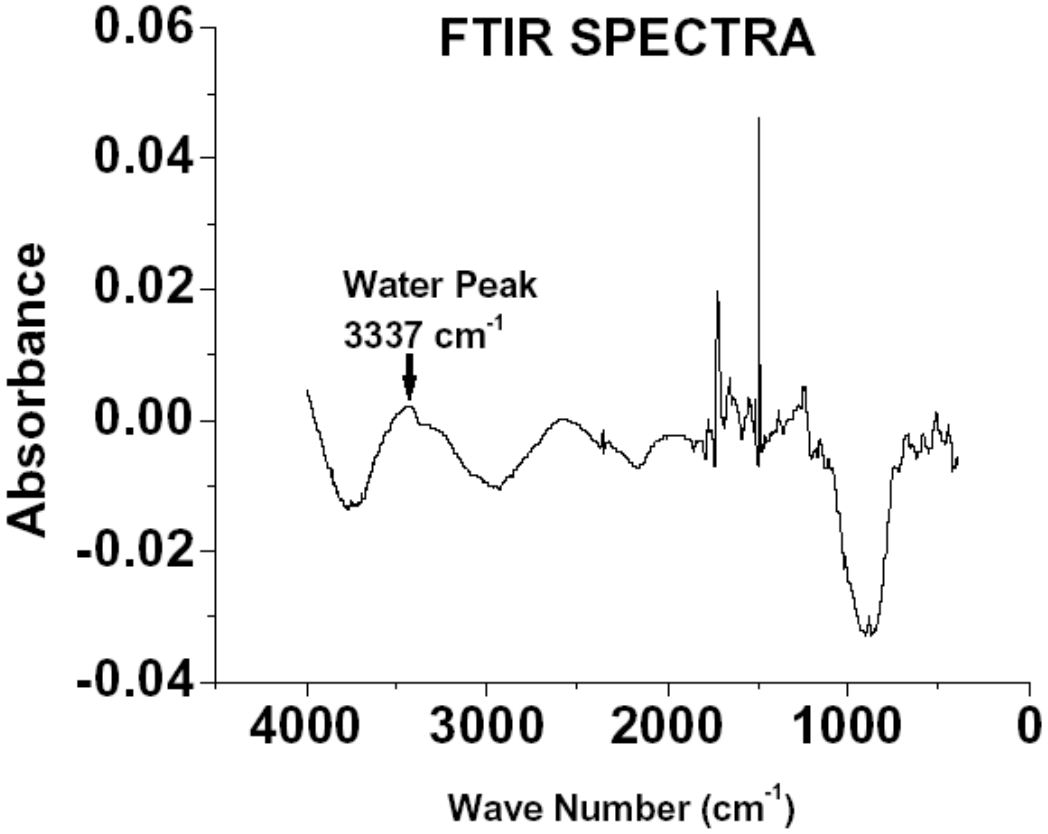

Figure 7. A typical FTIR spectrum showing the presence of water absorption peak corresponding to 3337 cm^{-1}.

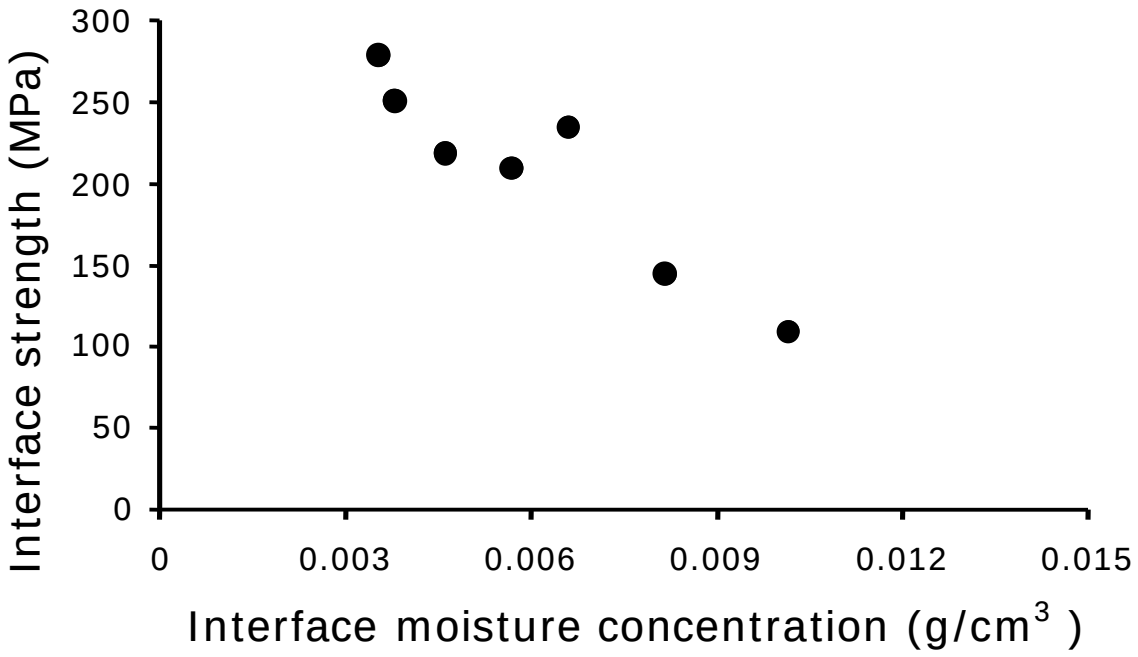

Figure 8. The effect of moisture content on the interface strength for samples in Groups 1 and 2, which were all exposed at 38°C. A linear fit identifies C_{crit}, an interface moisture concentration at which the strength will be reduced to zero.

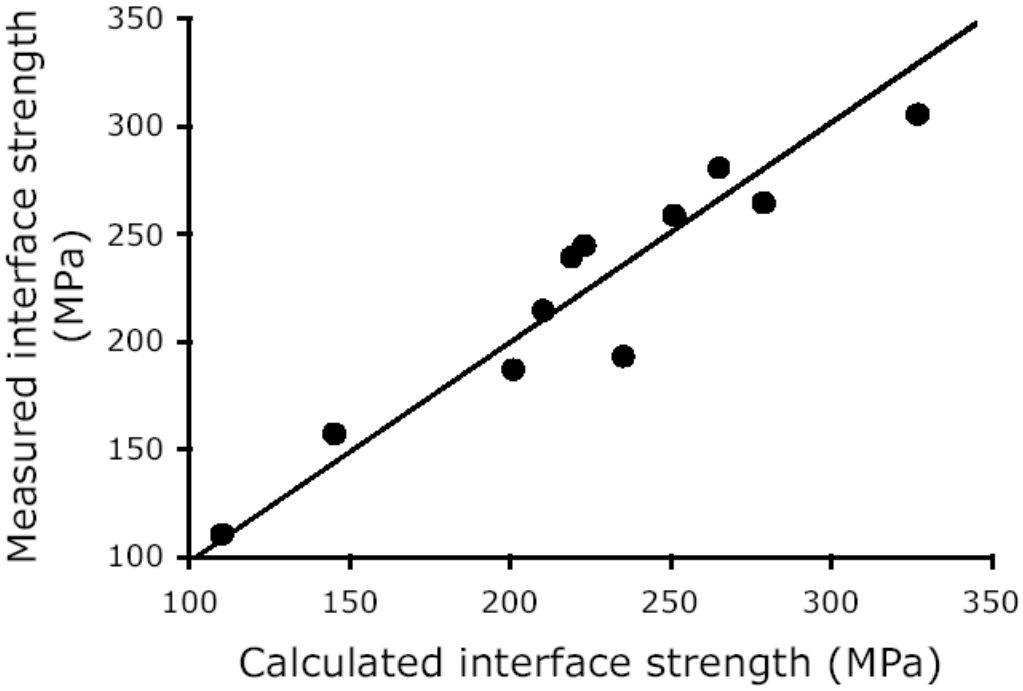

Figure 9. Plot of the measured interface strength versus calculated interface strength using Equation 1. The 45° line would match an exact fit between the measured and calculated strengths.

Figure 10. A schematic of the experimental process used for stiction release in MEMS devices.

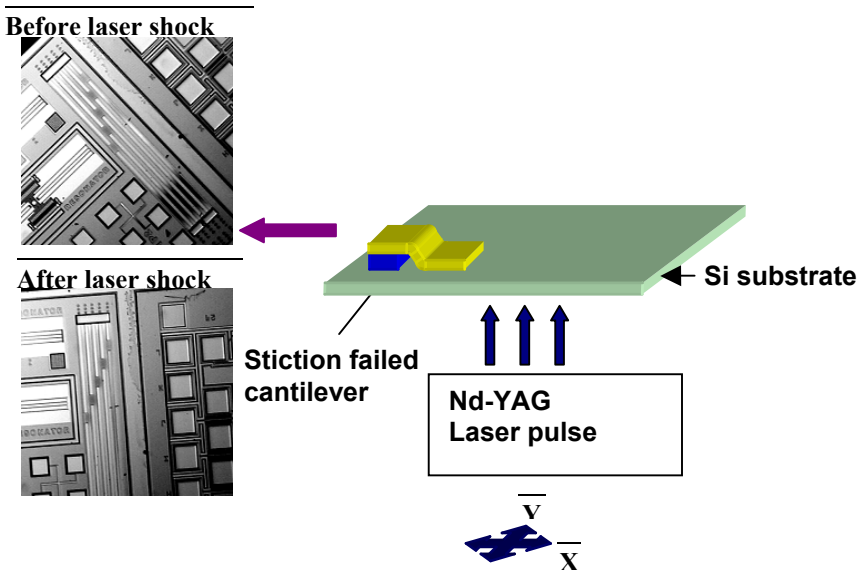

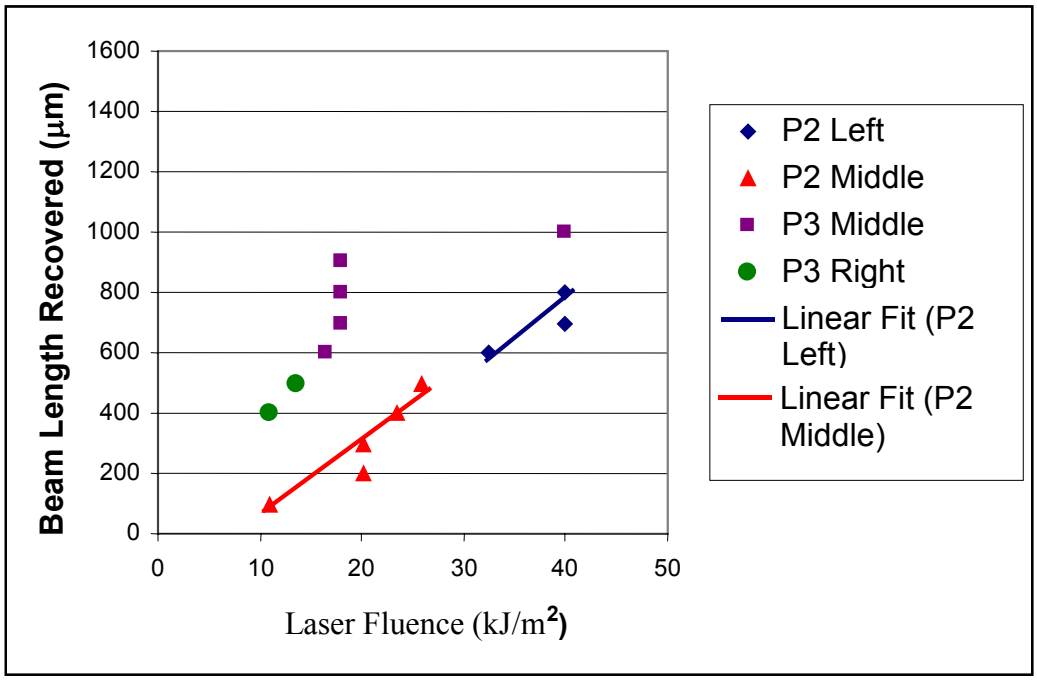

Figure 11. Quantitative data showing the laser fluence needed for releasing stiction failed beams.

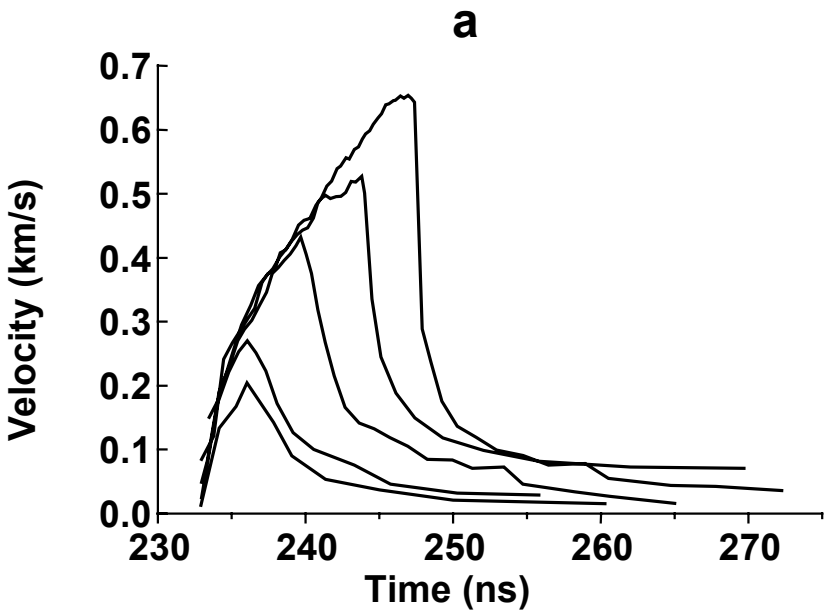

Figure 12. Series of stress pulse profiles with increasing laser fluence, measured in a soda lime glass.

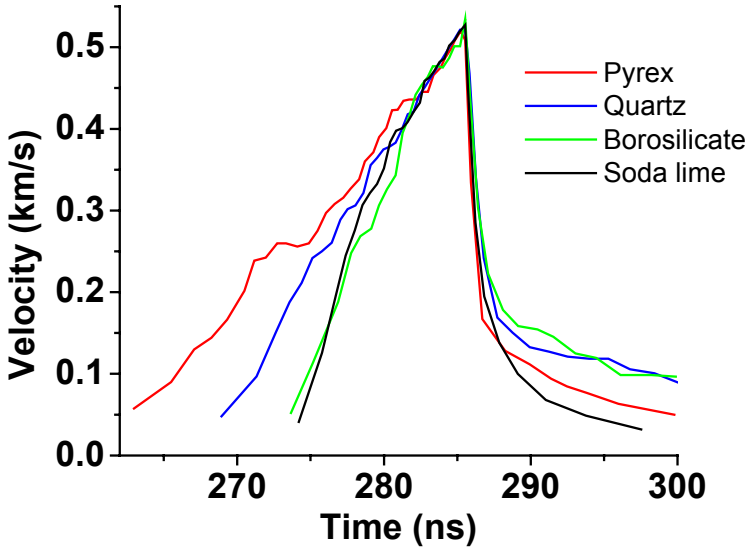

Figure 13. Stress wave profiles in various glasses.

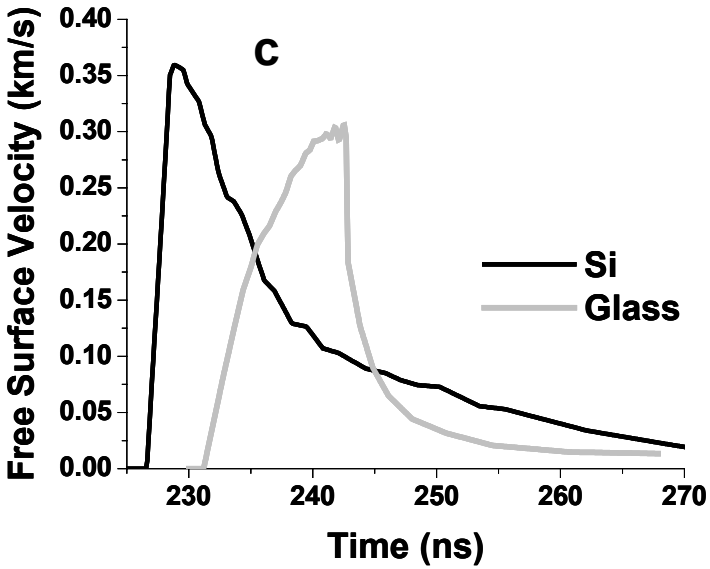

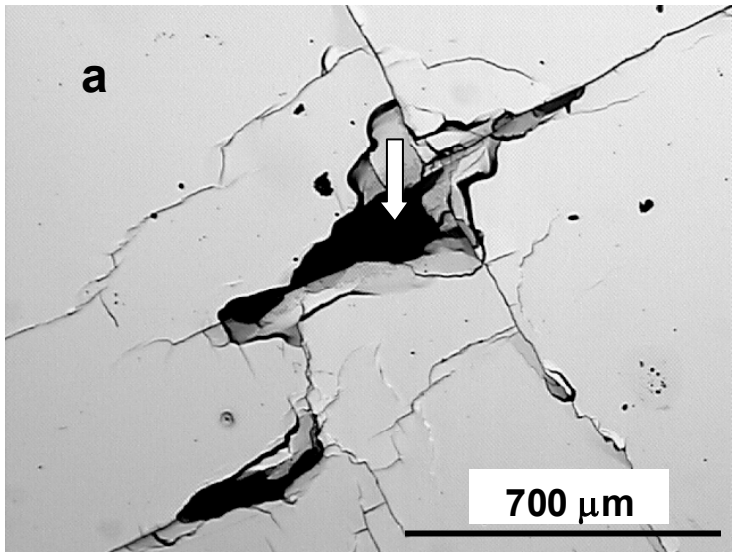

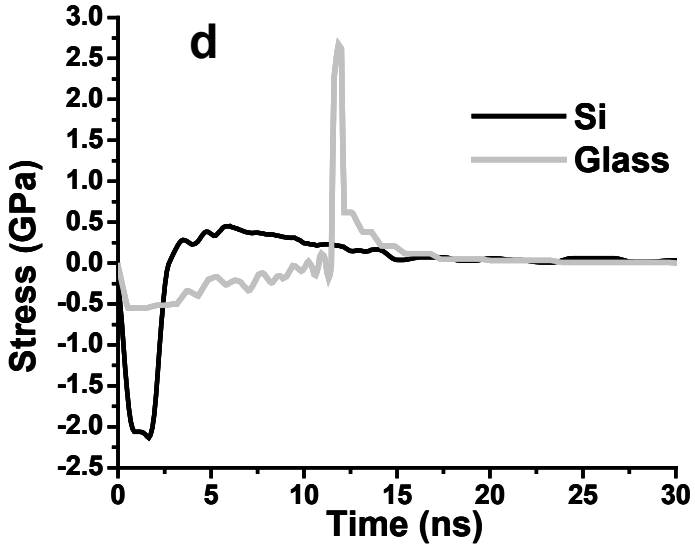

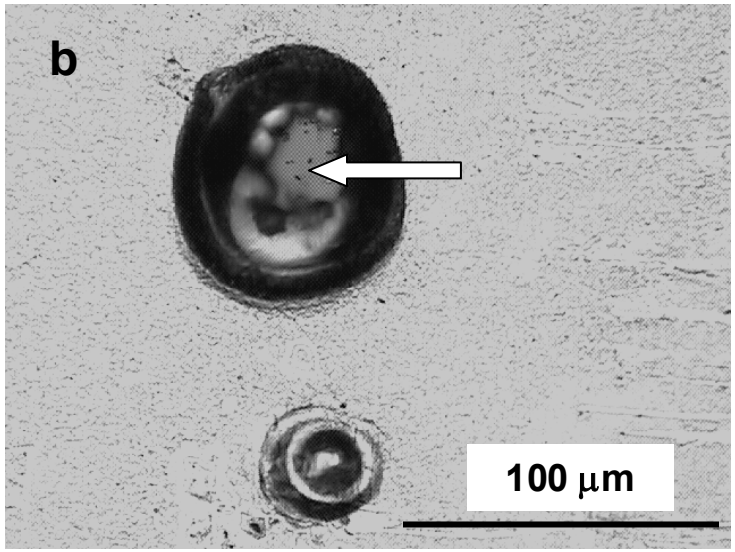

Figure 3. Failure in a Cu(140nm)/TiN(70nm)/Si system. (a) With no glass attached to the Si, the failure occurred cohesively inside the Si. (b) With glass-modified wave, failure was observed at the interface failure as shown by the arrow. The failure was determined to be specifically at the Cu/TiN interface.